



HAL
open science

Numerical study of turbulent cavitating flows in thermal regime

Eric Goncalves da Silva, Dia Zeidan

► **To cite this version:**

Eric Goncalves da Silva, Dia Zeidan. Numerical study of turbulent cavitating flows in thermal regime. International Journal of Numerical Methods for Heat and Fluid Flow, 2017, 27 (7), pp.1487-1503. 10.1108/HFF-05-2016-0202 . hal-01578647

HAL Id: hal-01578647

<https://hal.science/hal-01578647>

Submitted on 29 Aug 2017

HAL is a multi-disciplinary open access archive for the deposit and dissemination of scientific research documents, whether they are published or not. The documents may come from teaching and research institutions in France or abroad, or from public or private research centers.

L'archive ouverte pluridisciplinaire **HAL**, est destinée au dépôt et à la diffusion de documents scientifiques de niveau recherche, publiés ou non, émanant des établissements d'enseignement et de recherche français ou étrangers, des laboratoires publics ou privés.

Numerical study of turbulent cavitating flows in thermal regime

Eric Goncalves^a and Dia Zeidan^b

^a ISAE-ENSMA, Institut Pprime, UPR 3346 CNRS, Poitiers, France.

^b School of Basic Sciences and Humanities, German Jordanian University, Amman,
Jordan.

Abstract

Purpose The aim of this work is to quantify the relative importance of the turbulence modelling for cavitating flows in thermal regime. A comparison of various transport-equation turbulence models and a study of the influence of the turbulent Prandtl number appearing in the formulation of the turbulent heat flux are proposed. Numerical simulations are performed on a cavitating Venturi flow for which the running fluid is freon R-114 and results are compared with experimental data.

Design/methodology/approach A compressible, two-phase, one-fluid Navier-Stokes solver has been developed to investigate the behaviour of cavitation models including thermodynamic effects. The code is composed of three conservation laws for mixture variables (mass, momentum and total energy) and a supplementary transport equation for the volume fraction of gas. The mass transfer between phases is closed assuming its proportionality to the mixture velocity divergence.

Findings The influence of turbulence model as regard to the cooling effect due to the vaporization is weak. Only the $k - \varepsilon$ Jones-Launder model under-estimates the temperature drop. The amplitude of the wall temperature drop near the Venturi throat increases with the augmentation of the turbulent Prandtl number.

Originality The interaction between RANS turbulence closure and non isothermal phase transition is rarely studied. It is the first time such a study on the turbulent Prandtl number effect is reported in cavitating flows.

Keywords cavitation; thermodynamic effects; homogeneous model; RANS simulation; turbulence models; turbulent Prandtl number

1 Introduction

The turbopump design stages of liquid rocket engines requires an accurate prediction of the performance of cavitating cryogenic inducers involving thermodynamic effects. For cryogenic fluids, the liquid-vapour density ratio is lower than that of typical fluids (cold water) and consequently more liquid mass has to vaporize to sustain a cavity. Therefore evaporative cooling effects are more pronounced and the temperature of the liquid in the immediate vicinity of the liquid-vapour interface is depressed below the free-stream temperature. The temperature depression, negligible in cold water, is quite substantial. The local cooling effect delays the cavitation phenomenon and reduces the local vapour pressure of the fluid, which leads to a lower observed cavity pressure. Typically, this results in an improved mean performance of cryogenic pumps. Early studies about thermal effects were generally focused on obtaining correlations for temperature depression as a function of flow conditions and liquid properties. Classical methods include the B-factor theory (Stahl *et al.*, 1956) to characterize the sensitivity of fluids to thermodynamic effects. Another approach is based on the bubble dynamics model through the use of the Rayleigh-Plesset equation. This model is capable of handling either single bubbles or clouds of bubbles that grow and decrease through a pressure field (Fujikawa *et al.*, 2080). Yet, when thermal effects are involved, the liquid inertia becomes rapidly negligible and the evolution is controlled by the heat flux provided by the liquid at the bubble surface (Florschuetz and Chao, 1965, Prosperetti and Plesset, 1978).

A considerable literature exists on the simulations of two-phase fluid flow problems. See for example (Voller, 2016, Wang *et al.*, 2015, Liang *et al.*, 2014, Paniagua *et al.*, 2013, Daude and Galon, 2016, Zeidan, 2016, Zeidan *et al.*, 2014) and references therein. These simulations are mainly based on the widely used two-fluid model which is derived on the basis of averaging values for all the flow parameters and state variables ranging from seven to three equations. For instance, a seven-equation two-phase model has been proposed in, e.g. see (Saurel and Metayer, 2001) with velocity and pressure non-equilibrium where interfacial forces appear between phases developing momentum and energy exchange.

Another reduced five-equation model has been derived from a two-fluid model with the assumptions of velocity and pressure equilibrium (Kapila *et al.*, 2001). It is composed of four conservation laws: two for masses, one for the mixture momentum and one for the mixture energy. It is completed by an equation for a non-conservative quantity describing the flow topology, usually the void ratio. Such a model has been used for inviscid high speed cavitating applications (Saurel *et al.*, 2008, Rodio and Abgrall, 2015). By assuming the thermal equilibrium between phases, a four-equation model can be obtained. A very popular formulation, originally developed to simulate turbulent cavitating flows in cold water, has been adapted to cryogenic applications (Utturkar *et al.*, 2005, Tseng and Shyy, 2010, Huang *et al.*, 2014). It is composed by three conservation laws for mixture quantities (mass, momentum, energy) plus a mass equation for the vapour or liquid density including a cavitation source (different sets of models are presented in (Utturkar *et al.*, 2005)). Yet, this family of models are not thermodynamically well-posed and does not respect thermodynamic constraints such as mixture speed of sound conditions (Goncalves and Patella, 2011). With the assumption of complete thermodynamic equilibrium between phases (local temperature, pressure and free Gibbs enthalpy equality between phases), we obtain the 3-equation models or Homogeneous Equilibrium Models (HEM). An equation of state (EOS) is necessary to close the system. Different closure relations (tabulated EOS or combination of pure phase EOSs) that link the pressure to the thermodynamic variables have been proposed (Cooper, 1967, Clerc, 2000, Goncalves and Patella, 2010). The objective of this paper is to evaluate the sensitivity related to the choice of turbulence models on the cavitation prediction for liquid rocket engines. A canonical cavitating flow on a Venturi geometry is chosen for which the running fluid is freon R-114 ($C_2Cl_2F_4$). The cavitation model is based on a transport-equation for the void fraction in which the mass transfer between phases appear explicitly. This term is closed by assuming its proportionality with the velocity divergence (Goncalves, 2013, Goncalves and Charriere, 2014, Goncalves and Zeidan, 2016*a,b*). We investigate the thermal effects as regard to the temperature drop inside the cavitation pocket by testing the influence of (i) different transport-equation turbulence models associated with the Boussinesq assumption, (ii)

the turbulent heat flux through a turbulent Fourier law. The numerical simulations are compared with experimental data based on void ratio profiles and wall temperature depression. This paper is organized as follows. In Section 2, we present the cavitation model, the mass transfer closure relations and the mixture equation of states. Section 3 describes the Reynolds-Averaged Navier-Stokes formulation (RANS) with the turbulence modeling and the numerical schemes for the solving the model equations. A description of the Venturi case is given in Section 4. This is followed by simulation results demonstrating the influence of turbulence model. The last section is a conclusion.

2 Cavitation model

The homogeneous mixture approach is used to model two-phase flows. In addition, the phases are assumed to be in mechanical equilibrium: they share the same pressure P . Although the temperature-equalizing time is larger than the pressure and velocity relaxation times, as noted in (Kapila *et al.*, 2001), it is possible to consider a single-temperature model as an approximate model of flow if the difference of phase temperatures is not too big.

2.1 A four-equation single-temperature model

The model consists of three conservation laws for mixture quantities and an additional equation for the void ratio (Goncalves, 2013). We present below the inviscid one-dimensional

equations, expressed with the vector of variables $w = (\rho, \rho u, \rho E, \alpha)$:

$$\frac{\partial \rho}{\partial t} + \frac{\partial \rho u}{\partial x} = 0 \quad (1)$$

$$\frac{\partial(\rho u)}{\partial t} + \frac{\partial(\rho u^2 + P)}{\partial x} = 0 \quad (2)$$

$$\frac{\partial(\rho E)}{\partial t} + \frac{\partial(\rho u H)}{\partial x} = 0 \quad (3)$$

$$\frac{\partial \alpha}{\partial t} + u \frac{\partial \alpha}{\partial x} = K \frac{\partial u}{\partial x} + \frac{\dot{m}}{\rho_I} \quad (4)$$

$$K = \frac{\rho_l c_l^2 - \rho_v c_v^2}{\frac{\rho_l c_l^2}{1-\alpha} + \frac{\rho_v c_v^2}{\alpha}} \quad \text{and} \quad \frac{1}{\rho_I} = \frac{\frac{c_v^2}{\alpha} + \frac{c_l^2}{1-\alpha}}{\frac{\rho_l c_l^2}{1-\alpha} + \frac{\rho_v c_v^2}{\alpha}} \quad (5)$$

where $E = e + u^2/2$ and $H = h + u^2/2$ denote the mixture total energy and the mixture total enthalpy, respectively. The quantity K reflects the effects of changes in volume of each phase, ρ_I is the interfacial density, \dot{m} is the mass transfer between phases and c_k the speed of sound of the phase k .

2.2 Pure phase EOS

The liquid density ρ_l is assumed to be in its equilibrium state at the reference temperature: $\rho_l = \rho_l^{sat}(T_{ref})$. The vapour density ρ_v follows the stiffened gas EOS and varies with the temperature. The convex stiffened gas EOS relations are (see (Metayer *et al.*, 2004)):

$$P(\rho, e) = (\gamma - 1)\rho(e - q) - \gamma P_\infty \quad (6)$$

$$P(\rho, T) = \rho(\gamma - 1)C_v T - P_\infty \quad (7)$$

$$T(\rho, h) = \frac{h - q}{C_p} \quad (8)$$

where $\gamma = C_p/C_v$ is the heat capacity ratio, C_p and C_v are thermal capacities, q the energy of formation and P_∞ is a constant reference pressure. The speed of sound c is given by:

$$c^2 = \gamma \frac{P + P_\infty}{\rho} = (\gamma - 1)C_p T \quad (9)$$

The stiffened gas parameters for freon R-114 are given in Table 1.

	T_{ref} (K)	γ	P_∞ (Pa)	q (J/kg)	C_p (J/K.kg)	ρ^{sat} (kg/m ³)
liquid	293	1.1	3.835×10^7	-6.910×10^4	984	1470.3
vapour	293	1.07	0	1.424×10^5	700	13.52

Table 1: Parameters of the stiffened gas EOS for freon R-114 at saturation.

2.3 Closure relation for the mass transfer

By assuming that the mass transfer is proportional to the divergence of the velocity, it is possible to build a family of models (Goncalves, 2013, Goncalves and Charriere, 2014) in which the mass transfer is expressed as:

$$\dot{m} = \frac{\rho_l \rho_v}{\rho_l - \rho_v} \left(1 - \frac{c^2}{c_{wallis}^2} \right) \frac{\partial u}{\partial x} \quad (10)$$

where c_{wallis} is the propagation velocity of acoustic waves without mass transfer (Wallis, 1967). This speed of sound is expressed as a weighted harmonic mean of speeds of sound of each phase:

$$\frac{1}{\rho c_{wallis}^2} = \frac{\alpha}{\rho_v c_v^2} + \frac{1 - \alpha}{\rho_l c_l^2} \quad (11)$$

2.4 Mixture EOS

To close the system and to compute the mixture pressure and the mixture temperature, a equation of state for the mixture is necessary. A sinusoidal relation can be considered for the mixture (Goncalves and Patella, 2010). When the pressure is smaller than $P_{vap}(T) + \Delta P$, the following relationship applies:

$$P(\alpha, T) = P_{vap}(T) + \left(\frac{\rho_l^{sat} - \rho_v^{sat}}{2} \right) c_0^2 \sin^{-1}(1 - 2\alpha) \quad (12)$$

This EOS introduces a small non-equilibrium effect on the pressure quantified by the quantity ΔP . For a void ratio value of 0.5, the pressure is equal to the saturation pressure $P_{vap}(T)$ at the local temperature T . The saturation values ρ_l^{sat} and ρ_v^{sat} are evaluated at the reference temperature T_{ref} . The quantity c_0 , which has the dimension of a velocity,

is a parameter of the model. The pressure continuity between the liquid and the mixture is given by:

$$\frac{\pi}{2} \frac{\rho_l^{sat} - \rho_v^{sat}}{2} c_0^2 = \rho_l^{sat} (\gamma_l - 1) C_{vl} T_{ref} - P_\infty^l - P_{vap}(T_{ref}) \quad (13)$$

This relation determines c_0 for given values of saturation conditions. In the present study, $c_0 = 0.74$ m/s.

We assume that the vaporization pressure varies linearly with the temperature:

$$P_{vap}(T) = P_{vap}(T_{ref}) + \frac{dP_{vap}}{dT}(T - T_{ref}) \quad (14)$$

The constant quantity dP_{vap}/dT is evaluated using a thermodynamic table around a reference temperature. In the present study, $dP_{vap}/dT = 5900$ Pa/K.

The speed of sound in the mixture can be written as (Goncalves and Patella, 2010):

$$c^2 = \frac{\frac{\rho_v \rho_l}{\rho(\rho_l - \rho_v)} (h_v - h_l) \frac{dP_{vap}}{dT} + \rho C_p(Y) c_T^2}{\rho C_p(Y) - \frac{dP_{vap}}{dT}} \quad (15)$$

$$C_p(Y) = Y C_{pv} + (1 - Y) C_{pl} \quad (16)$$

$$c_T^2 = \left(\frac{\partial P}{\partial \rho} \right)_s = \left(\frac{\partial P}{\partial \rho} \right)_T = \frac{c_0^2}{2\sqrt{\alpha(1-\alpha)}} \quad (17)$$

Where c_T is the isothermal speed of sound (i.e. when $dP_{vap}/dT=0$) and $Y = \alpha \rho_v / \rho$ is the vapour mass fraction. The four-equation system is hyperbolic with eigenvalues: $\lambda_1 = u - c$, $\lambda_{2,3} = u$ and $\lambda_4 = u + c$.

Properties of the EOS as regard to both convexity and mixture speed of sound conditions have been studied in (Goncalves and Patella, 2010).

3 Reynolds averaged Navier-Stokes equations

For turbulent computations, the compressible one-fluid RANS equations are used, coupled with a one- or two-equation turbulence model. These equations can be expressed as:

$$\frac{\partial w}{\partial t} + \text{div}(F_c - F_v) = S \quad (18)$$

$$w = \begin{pmatrix} \rho \\ \rho \vec{V} \\ \rho E \\ \alpha \\ \rho k \\ \rho \Psi \end{pmatrix} ; \quad F_c = \begin{pmatrix} \rho \vec{V} \\ \rho \vec{V} \otimes \vec{V} + p \bar{I} \\ (\rho E + p) \vec{V} \\ \alpha \vec{V} \\ \rho k \vec{V} \\ \rho \Psi \vec{V} \end{pmatrix} ; \quad F_v = \begin{pmatrix} 0 \\ \overline{\overline{\tau^v}} + \overline{\overline{\tau^t}} \\ (\overline{\overline{\tau^v}} + \overline{\overline{\tau^t}}) \cdot \vec{V} - Q^v - Q^t \\ 0 \\ (\mu + \mu_t / \sigma_k) \text{grad } k \\ (\mu + \mu_t / \sigma_\Psi) \text{grad } \Psi \end{pmatrix}$$

where w denotes the conservative variables and the void ratio, F_c and F_v the convective and viscous flux densities and S the source terms, which concern the void ratio equation and the turbulent transport equation. k is the mixture turbulent kinetic energy and Ψ is a turbulent variable. The exact expression of the eddy-viscosity μ_t and the source terms depend on the turbulence model, as well as the constants σ_k and σ_Ψ .

The total stress tensor $\overline{\overline{\tau}}$ is evaluated using the Stokes hypothesis, Newton's law and the Boussinesq assumption. The total heat flux vector Q is obtained from the Fourier law involving a turbulent thermal conductivity λ_t .

$$\begin{aligned} \overline{\overline{\tau}} &= \overline{\overline{\tau^v}} + \overline{\overline{\tau^t}} = (\mu + \mu_t) \left[(\text{grad } \vec{V} + (\text{grad } \vec{V})^t) - \frac{2}{3} (\text{div } \vec{V}) \bar{I} \right] + \frac{2}{3} \rho k \bar{I} \\ Q &= Q^v + Q^t = -(\lambda + \lambda_t) \text{grad } T \end{aligned} \quad (19)$$

In the pure liquid, the viscosity is determined by an exponential law and, in pure vapour, the viscosity follows the Sutherland law. The mixture viscosity is defined as the arithmetic mean of the liquid and vapour viscosities:

$$\mu_l(T) = \mu_{0_l} \exp(B/T) \quad (20)$$

$$\mu_v(T) = \mu_{0_v} \sqrt{\frac{T}{293}} \frac{1 + T_S/293}{1 + T_S/T} \quad (21)$$

$$\mu(T, \alpha) = \alpha \mu_v(T) + (1 - \alpha) \mu_l(T) \quad (22)$$

where μ_{0_l} , μ_{0_v} , B and T_S are constant parameters.

The mixture thermal conductivity λ is also defined as the arithmetic mean of the

liquid and vapour values:

$$\lambda(\alpha, T) = \alpha \frac{\mu_v(T)C_{p_v}}{P_{r_v}} + (1 - \alpha) \frac{\mu_l(T)C_{p_l}}{P_{r_l}} \quad (23)$$

3.1 Wall modelling

For the modelling of flow close to the wall, a two-layer wall law approach is used (Goncalves and Houdeville, 2001):

$$\begin{aligned} u^+ &= y^+ && \text{if } y^+ < 11.13 \\ u^+ &= \frac{1}{\kappa} \ln y^+ + 5.25 && \text{if } y^+ > 11.13 \\ u^+ &= \frac{\kappa u}{U_\tau} && ; \quad y^+ = \frac{y U_\tau}{\nu_w} \quad ; \quad U_\tau^2 = \frac{\tau_w}{\rho_w} \end{aligned} \quad (24)$$

where $\kappa = 0.41$ is the von Karman constant and the subscript 'w' is used for a wall value. We assume that wall functions are similar in a two-phase flow and in a single-phase flow. This assumption have been studied in (Goncalves and Decaix, 2012) and comparisons were proposed with a thin boundary layer approach.

At the wall, an adiabatic condition is imposed. Gradients of temperature and pressure are assumed to be null. For the void ratio wall value, we use the following formulation:

$$\alpha_w = \frac{\rho_w - \rho_l^{sat}(T_{ref})}{\rho_v(T_w) - \rho_l^{sat}(T_{ref})} \quad \text{with} \quad \rho_v(T_w) = \frac{P_w}{C_{v_v}(\gamma_v - 1)T_w} \quad (25)$$

3.2 Turbulence models

A comparison with various transport-equation turbulence models is proposed. We consider five models: the one-equation Spalart-Allmaras model (SA) (Spalart and Allmaras, 1994), the Jones-Launder $k - \varepsilon$ model (KE) (Jones and Launder, 1972), the Smith $k - \ell$ model (KL) (Smith, 1994), the Wilcox $k - \omega$ model (KO) (Wilcox, 1988) and the Menter SST $k - \omega$ model (SST) (Menter, 1994).

3.3 Turbulent heat flux

We introduce a constant turbulent Prandtl number hypothesis. The mixture turbulent thermal conductivity is given by the arithmetic mean of the liquid and vapour values:

$$\lambda_t = \alpha\lambda_v^t + (1 - \alpha)\lambda_l^t = \alpha\frac{\mu_t C_{pv}}{P_{rt}} + (1 - \alpha)\frac{\mu_t C_{pl}}{P_{rt}} \simeq \frac{\mu_t C_p(Y)}{P_{rt}} \quad (26)$$

where the turbulent Prandtl number P_{rt} is usually set to 1, that is to say the momentum and thermal eddy diffusivities are in the same order of magnitude. For two-dimensional boundary layer, this number is evaluated by

$$P_{rt} = \frac{\nu_t}{\alpha_t} = \frac{\overline{u'v'}\frac{\partial T}{\partial y}}{\overline{v'T'}\frac{\partial u}{\partial y}} \quad (27)$$

A large quantity of experimental, analytical and numerical works have been devoted to the evaluation of this number in the near-wall region of single-phase boundary layer (see review by (Kays, 1994)). A clear lack of agreement appears in the literature. For a two-phase boundary layer involving phase transition, the question is totally open. We propose to test different values of P_{rt} from 0.25 to 1.5.

3.4 Numerical methods

The numerical simulations are carried out using an implicit CFD code based on a finite-volume discretization. For the mean flow, the convective flux density vector on a cell face is computed with the Jameson-Schmidt-Turkel scheme (Jameson *et al.*, 1981). The artificial viscosity includes a second-order dissipation term D_2 and a fourth-order dissipation term D_4 , which involve two tunable parameters. The viscous terms are discretized by a second-order space-centered scheme. For the turbulence transport equations, the upwind Roe scheme (Roe, 1981) is used to obtain a more robust method. The second-order accuracy is obtained by introducing a flux-limited dissipation. The numerical treatment of boundary conditions is based on the use of the characteristic relationships. More details are given in (Goncalves, 2013).

4 Application: the Venturi geometry

4.1 Experimental conditions

The freon R-114 experimental facility of the CREMHyG is a closed loop operating with a reference pressure, obtained by pressurizing a tank with nitrogen gas. The loop is fitted with a test section having the shape of a two-dimensional Venturi, characterized by a convergence angle of 4.3° and a divergence angle of 4° (Fig. 1). The edge forming the throat of the Venturi is used to fix the separation point of the cavitation cavity. This geometry is equipped with three probing holes to take various measurements. Optical probes and micro-thermocouples are used to evaluate the local void ratio and the wall temperature, respectively. For this geometry, the selected operation point is characterized by the following physical parameters (Fruman *et al.*, 1999):

- the inlet velocity $V_{inlet} = 14.4$ m/s;
- the reference temperature $T_{ref} = 293$ K;
- the reference length $L_{ref} = 0.252$ mm, corresponding to the chord of a blade turbomachinery;
- the Reynolds number $Re_{L_{ref}} = \frac{V_{inlet} \times L_{ref}}{\nu(T_{ref})} = 18.4 \times 10^6$;
- the cavitation parameter in the inlet section $\sigma_{inlet} = \frac{P_{inlet} - P_{vap}(T_{ref})}{0.5\rho V_{inlet}^2} \simeq 0.55$.

With these parameters, a cavity length L_{cav} around 80 mm was obtained, with a relatively stable aspect.

A simple heat balance between the two phases can estimate the scale of temperature difference ΔT^* caused by thermal effects.

$$\Delta T^* = \frac{\rho_v L_{vap}}{\rho_l C_{pl}} \quad (28)$$

where L_{vap} is the latent heat. Values of this temperature difference are given in Table 2 for water, freon R-114 and liquid hydrogen LH_2 in cryogenic conditions. Freon R-114 provides a similar ΔT^* at room temperature in comparison with LH_2 and is used as a substitute fluid for turbopump applications.

fluid	T_{ref} (K)	ρ_L (kg/m ³)	ρ_V (kg/m ³)	P_{vap} (Pa)	$\frac{dP_{vap}}{dT}$ (Pa/K)	ΔT^* (K)
water	293	998	0.02	2339	143	0.01
R-114	293	1470.3	13.52	181100	5900	1.22
LH2	21	70.0	1.62	124720	35300	1.01
LH2	21	67.4	2.60	209320	50000	1.41

Table 2: Thermodynamic properties of different fluids at saturation.

4.2 Computational parameters and mesh

The grid is a H-type topology. The mesh contains 251 nodes in the flow direction and 77 in the orthogonal direction. A special contraction is applied in the main flow direction just after the throat to better simulate the two-phase flow area (see Fig. 2). $y+$ values in first adjacent cells to walls vary between 35 to 50 for a non cavitating simulation.

All cavitating simulations are steady computations, which are started from the non cavitating numerical solution. Computations have been performed with a CFL number equal to 0.5 and dissipation parameters equal to 1 and 0.045.

4.3 Influence of the turbulence model

Different calculations were performed in order to obtain a cavitation sheet with a length close to 80 mm. Comparisons between different cavitation models have been presented in (Goncalves and Charriere, 2014) using the Spalart-Allmaras turbulence model. In the following, we study the turbulence model influence.

A qualitative view of the cavitation pocket attached to the throat is presented in Figure 3 with the void ratio field (top) and the temperature deficit $T - T_{ref}$ (K) (down). Results have been obtained using the $k - \omega$ SST Menter and the $k - \varepsilon$ Jones-Launder models. The cooling effect due to the vaporization process is clearly observed (negative values). In the recompression area, a warming effect is exhibited as observed previously

in (Goncalves, 2014) using the Spalart-Allmaras model. Locally, the temperature exceeds the freestream temperature and values reach more than 5 K. It is certainly due to the collapse of bubbles which causes the rapid recuperation of the temperature, as related by experimental measurements using infra-red thermography (Petkovsek and Dular, 2013). Such a phenomenon is predicted by all simulations with the five considered turbulence models. The qualitative view is quite similar for all simulations.

Complementary analyses concern local void ratio profiles inside the cavity and the wall temperature depression. The experimental void ratio profiles are obtained with a post processing algorithm from the signal of the optical probe (Fruman *et al.*, 1999). Figure 4 (on the left) illustrates the numerical void ratio obtained with the five turbulence models in comparison with the measurements at stations 1 to 3. We clearly observe that numerical results are quite superimposed. As regard to the wall value of the void ratio, a large discrepancy appears: the numerical wall values are largely over-predicted in comparison with the experimental data at stations 2 and 3. Moreover, the decrease of the void ratio close to the wall is absolutely not reproduced. This behaviour is probably due to the considered wall condition for the void ratio (equation 25).

For the analysis of the flow, we added a numerical probe inside the cavity at abscissa $x = 74$ mm named station 5. The temperature depression $T_{ref} - T$ at stations 1, 3 and 5 is plotted in Figure 4 (on the right) for the five turbulence models. The cooling effect is more pronounced at station 1, close to the Venturi throat. The shape of the profiles is quite similar for all simulations. Near the wall, small discrepancies are noticeable at stations 1 and 2. The wall temperature depression at station 1 is about 2.2 K (± 0.2 K) for the experimental data. Except the under-estimation provided by the Jones-Launder model (around 1.8 K), results are in very good agreement with the measurement. At station 2, similarly the Jones-Launder simulation provides a lower temperature drop in comparison with other models. Finally, at station 5, in the end part of the cavitation pocket, all models provide similar profiles. We note that the $k - \varepsilon$ model also predicted the highest void ratio wall values at stations 1 to 3.

To investigate the effect of turbulence models, profiles of viscosity ratio μ_t/μ (on the left) and thermal conductivity ratio λ_t/λ (on the right) are plotted in Figure 5 at stations 1 and 3 for the five turbulence models. Globally, discrepancies appear on the thickness of profiles and on the maximum values. The Jones-Launder model provides the thinnest profiles and the lowest values. On the contrary, the Smith $k - \ell$ model gives the highest values but it is not associated to a larger temperature drop.

4.4 Influence of the turbulent Prandtl number

As regard to the previous study, the Spalart-Allmaras model is chosen for all simulations. Different values of the turbulent Prandtl number are tested from 0.25 to 1.5. With a small value of P_{rt} , the thermal eddy diffusivity is faster than the momentum eddy diffusivity and a reduction of the thermal amplitude is expected.

First, a qualitative view of the cavitation pocket is illustrated in Figure 6 where the void ratio and temperature deficit fields are plotted. Three simulations are compared: $P_{rt} = 1.5$ (top), $P_{rt} = 1$ (middle) and $P_{rt} = 0.25$ (down). No clear discrepancies are put in evidence between simulations.

Secondly, the void ratio profiles at station 1 to 3 are presented in the left part of Figure 7. Using the smallest value $P_{rt} = 0.25$, the thickness of the cavity is a little reduced, especially at station 3. For the highest value $P_{rt} = 1.5$, the wall value is more important (around 75%) and the S-shape at station 3 is not predicted. For the intermediate values, profiles are quite similar.

Profiles of temperature depression $T_{ref} - T$ (K) at stations 1, 3 and 5 are plotted in the right part of Figure 7. At station 1, discrepancies are noticeable for the wall temperature depression. Higher is the turbulent Prandtl number, stronger is the temperature depression. Using the highest value $P_{rt} = 1.5$, the wall temperature difference reaches 2.5 K.

At stations 3 and 5, results are relatively similar. A small discrepancy appears on the maximum value at the interface of the cavitation pocket.

Complementary analyses are proposed for turbulent quantities. The viscosity ratio μ_t/μ and the thermal conductivity ratio λ_t/λ are plotted in Figure 8 for different values of P_{rt} . Viscosity ratio profiles are quite similar. The conductivity ratio profiles show large difference. The hierarchy between the five values of P_{rt} is well illustrated. The maximum ratio obtained with the smallest value $P_{rt} = 0.25$ is around 4.7 times the value predicted for the case $P_{rt} = 1$. For the case $P_{rt} = 1.5$, the augmentation is around a factor 1.4. The conductivity ratio is not directly proportional to the viscosity ratio through the Prandtl numbers in two-phase flow.

Finally, the wall temperature depression $T_{ref} - T$ (K) is presented in Figure 9 along the Venturi divergent function of the dimensionless abscissa $x^* = (x - x_{throat})/L_{cav}$. The experimental value corresponds to the wall measurement at station 1. Close to the throat, for $x^* \leq 0.1$, we observe a peak of the temperature depression followed by a decrease along the wall up to the closure part of the cavity. As observed on the temperature profile at station 1, this peak is more pronounced for the highest value $P_{rt} = 1.5$. From the abscissa $x^* = 0.2$, all results are quite superimposed. At the closure part of cavities, discrepancies are noticeable due to the fact that the cavity length L_{cav} is not exactly the same for all simulations. Negative values of the quantity $T_{ref} - T$ illustrate the warming effect in the recompression area.

5 Conclusion

One-fluid single-temperature RANS simulations were performed to study cavitation pockets developing along a Venturi geometry in which the working fluid is freon R-114. An investigation of the influence of various transport-equation turbulence models and the turbulent Prandtl number was led. Numerical results have been compared with experimental data, especially as regard to the cooling effect due to the vaporization process.

These investigations showed globally the weak effect of the turbulence model, only the $k - \varepsilon$ model provided a smaller temperature depression in comparison with other models. It is difficult to explain this behaviour. The physical mechanisms involved are not clear and the interaction between heat and mass transfers in a turbulent boundary layer remain challenging to model. Similarly, the influence of the turbulent Prandtl number is rather small. The amplitude of the wall temperature drop is modified near the throat and increases with the augmentation of P_{rt} .

Additional works are in progress to pursue comparative analyses and to develop 2-temperature models. Moreover, further experimental cavitating works concerning local measurements in thermosensitive fluid are capital to allow model calibration and validation.

References

- Clerc, S. (2000), ‘Numerical simulation of the homogeneous equilibrium model for two-phase flows’, *Journal of Computational Physics* **161**(1), 354–375.
- Cooper, P. (1967), ‘Analysis of single and two-phase flow in turbopump inducers’, *Journal of Fluids Engineering* **89**, 577–588.
- Daude, F. and Galon, P. (2016), ‘On the computation of the Baer-Nunziato model using ALE formulation with HLL- and HLLC-type solvers towards fluidstructure interactions’, *Journal of Computational Physics* **304**, 189–230.
- Florschuetz, L. and Chao, B. (1965), ‘On the mechanics of vapor bubble collapse’, *Journal of Heat Transfer* **87**, 209–220.
- Fruman, D., Reboud, J. and Stutz, B. (1999), ‘Estimation of thermal effects in cavitation of thermosensible liquids’, *Int. Journal of Heat and Mass Transfer* (42), 3195–3204.
- Fujikawa, S., Okuda, M. and Akamatsu, T. (2080), ‘Non-equilibrium vapour condensation on a shock-tube endwall behind a reflected shock wave’, *Journal of Fluid Mechanics* (183), 293–324.
- Goncalves, E. (2013), ‘Numerical study of expansion tube problems: Toward the simulation of cavitation’, *Computers & Fluids* **72**, 1–19.
- Goncalves, E. (2014), ‘Modeling for non isothermal cavitation using 4-equation models’, *International Journal of Heat and Mass Transfer* **76**, 247–262.
- Goncalves, E. and Charriere, B. (2014), ‘Modelling for isothermal cavitation with a four-equation model’, *International Journal of Multiphase Flow* **59**, 54–72.
- Goncalves, E. and Decaix, J. (2012), ‘Wall model and mesh influence study for partial cavities’, *European Journal of Mechanics B/Fluids* **31**(1), 12–29.

- Goncalves, E. and Houdeville, R. (2001), ‘Reassessment of the wall functions approach for RANS computations’, *Aerospace Science and Technology* **5**, 1–14.
- Goncalves, E. and Patella, R. F. (2010), ‘Numerical study of cavitating flows with thermodynamic effect’, *Computers & Fluids* **39**(1), 99–113.
- Goncalves, E. and Patella, R. F. (2011), ‘Constraints on equation of state for cavitating flows with thermodynamic effects’, *Applied Math. and Computation* **217**, 5095–5102.
- Goncalves, E. and Zeidan, D. (2016a), ‘Numerical simulation of unsteady cavitation in liquid hydrogen flows’, *Int. J. of Engineering Systems Modelling and Simulation*.
- Goncalves, E. and Zeidan, D. (2016b), Study of thermal effects in a cavitating venturi flow, *in* ‘The 9th International Conference on Thermal Engineering Theory and Applications, March 24-26, 2016, Abu Dhabi, UAE’.
- Huang, B., Wu, Q. and Wang, G. (2014), ‘Numerical investigation of cavitating flow in liquid hydrogen’, *Int. Journal of Hydrogen Energy* **39**, 1698–1709.
- Jameson, A., Schmidt, W. and Turkel, E. (1981), Numerical solution of the Euler equations by finite volume methods using Runge-Kutta time stepping schemes, *in* ‘AIAA Paper 81–1259’.
- Jones, W. and Launder, B. (1972), ‘The prediction of laminarization with a two-equation model of turbulence’, *Int. J. Heat and Mass Transfer* **15**, 301–314.
- Kapila, A., Menikoff, R., Bdzil, J., Son, S. and Stewart, D. (2001), ‘Two-phase modeling of deflagration-to-detonation transition in granular materials: reduced equations’, *Physics of fluids* **13**(10), 3002–3024.
- Kays, W. (1994), ‘Turbulent Prandtl number - where are we?’, *ASME Journal of Heat Transfer* **116**, 284–295.
- Liang, S., Liu, W. and Yuan, L. (2014), ‘Solving seven-equation model for compressible two-phase flow using multiple GPUs’, *Computers & Fluids* **99**, 156–171.

- Menter, F. (1994), ‘Two-equation eddy-viscosity turbulence models for engineering applications’, *AIAA Journal* **32**(8), 1598–1605.
- Metayer, O. L., Massoni, J. and Saurel, R. (2004), ‘Elaborating equations of state of a liquid and its vapor for two-phase flow models’, *Int. Journal of Thermal Sciences* **43**, 265–276.
- Paniagua, G., Lavagnoli, S., Verstraete, T., Mahmoudi, W. and Benarama, T. (2013), ‘Aero-design of transonic LH2 and LOx contra rotating turbopumps in an expander rocket engine’, *International Journal of Numerical Methods for Heat & Fluid Flow* **23**, 575–587.
- Petkovsek, M. and Dular, M. (2013), ‘IR measurements of the thermodynamic effects in cavitating flow’, *International Journal of Heat and Fluid Flow* **44**, 756–763.
- Prosperetti, A. and Plesset, M. (1978), ‘Vapour-bubble growth in a superheated liquid’, *Journal of Fluid Mechanics* **85**, 349–368.
- Rodio, M. and Abgrall, R. (2015), ‘An innovative phase transition modeling for reproducing cavitation through a five-equation model and theoretical generalization to six and seven-equation models’, *Int. Journal of Heat and Mass Transfer* **89**, 1386–1401.
- Roe, P. (1981), ‘Approximate Riemann solvers, parameters vectors, and difference schemes’, *Journal of Computational Physics* **43**, 357–372.
- Saurel, R. and Metayer, O. L. (2001), ‘A multiphase model for compressible flows with interfaces, shocks, detonation waves and cavitation’, *Journal of Fluid Mechanics* **431**, 239–271.
- Saurel, R., Petitpas, F. and Abgrall, R. (2008), ‘Modelling phase transition in metastable liquids: application to cavitating and flashing flows’, *Journal of Fluid Mechanics* **607**, 313–350.

- Smith, B. (1994), A near wall model for the $k - l$ two equation turbulence model, in ‘AIAA 94-2386, 25th Fluid Dynamics Conference – Colorado Springs, Colorado’.
- Spalart, P. and Allmaras, S. (1994), ‘A one-equation turbulence model for aerodynamic flows’, *La Recherche Aéronautique* (1), 5–21.
- Stahl, H., Stepanoff, A. and Phillipsburg, N. (1956), ‘Thermodynamic aspects of cavitation in centrifugal pumps’, *Journal of Fluids Engineering* **78**, 1691–1693.
- Tseng, C. and Shyy, W. (2010), ‘Modeling for isothermal and cryogenic cavitation’, *Int. Journal of Heat and Mass Transfer* **53**, 513–525.
- Utturkar, Y., Wu, J., Wang, G. and Shyy, W. (2005), ‘Recent progress in modelling of cryogenic cavitation for liquid rocket propulsion’, *Progress in Aerospace Sciences* **41**, 558–608.
- Voller, V. (2016), ‘Computations of anomalous phase change’, *International Journal of Numerical Methods for Heat & Fluid Flow* **26**, 624–638.
- Wallis, G. (1967), ‘One-dimensional two-phase flow’, New York: McGraw-Hill.
- Wang, J., Wang, Y., Liu, H., Huang, H. and Jiang, L. (2015), ‘An improved turbulence model for predicting unsteady cavitating flows in centrifugal pump’, *International Journal of Numerical Methods for Heat & Fluid Flow* **25**, 1198–1213.
- Wilcox, D. (1988), ‘Reassessment of the scale-determining equation for advanced turbulence models’, *AIAA Journal* **26**(11), 1299–1310.
- Zeidan, D. (2016), ‘Assessment of mixture two-phase flow equations for volcanic flows using Godunov-type methods’, *Applied Mathematics and Computation* **272**, 707–719.
- Zeidan, D., Touma, R. and Slaouti, A. (2014), ‘Application of a thermodynamically compatible two-phase flow model to the high-resolution simulations of compressible gas-magma flow’, *International Journal for Numerical Methods in Fluids* **76**, 312–330.

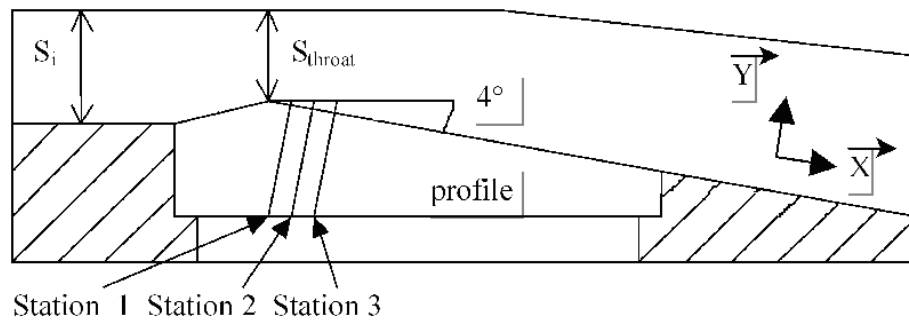


Figure 1: Schematic view of the Venturi profile.

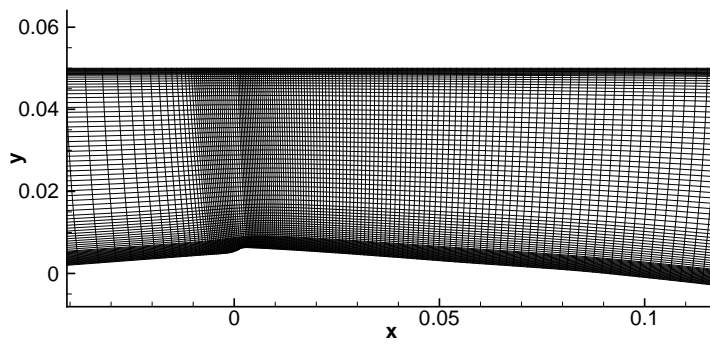


Figure 2: Enlargement of the mesh near the throat.

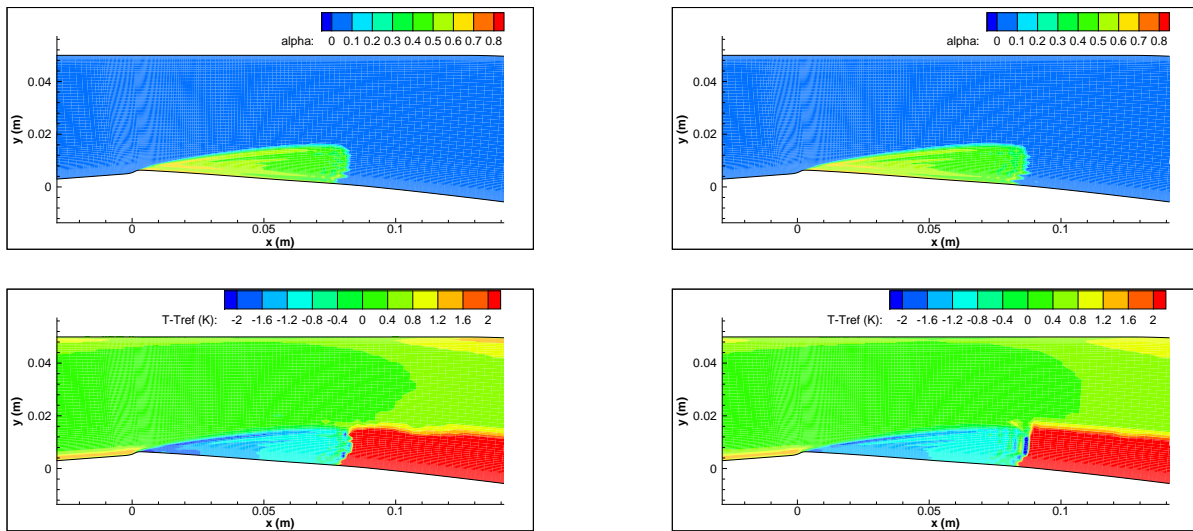


Figure 3: Void ratio and temperature difference $T - T_{ref}$ (K) contours, SST Menter model (left) and $k - \varepsilon$ Jones-Launder model (right).

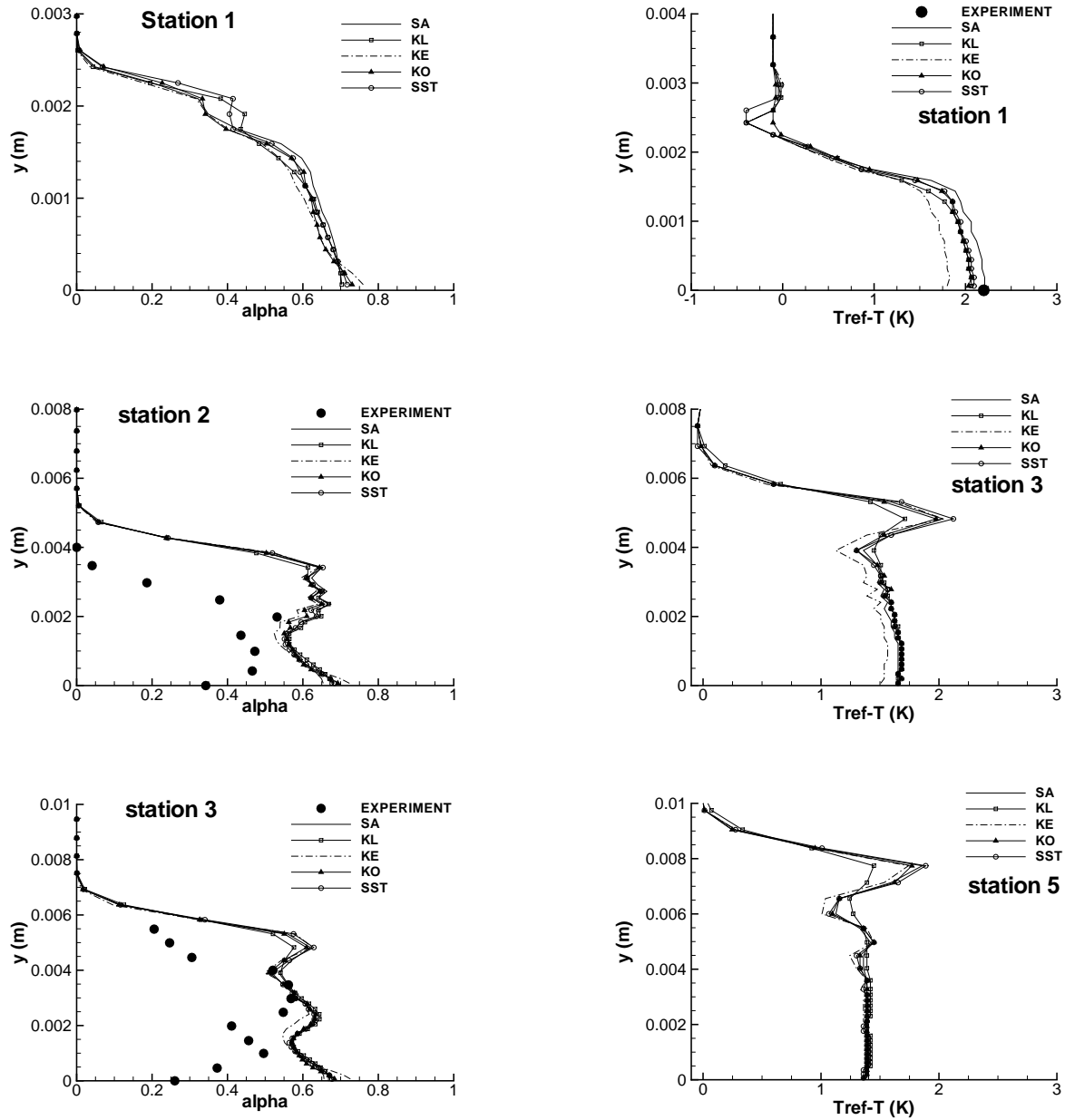


Figure 4: Profiles of void ratio and temperature drop $T_{ref} - T$ at different stations, turbulence model influence.

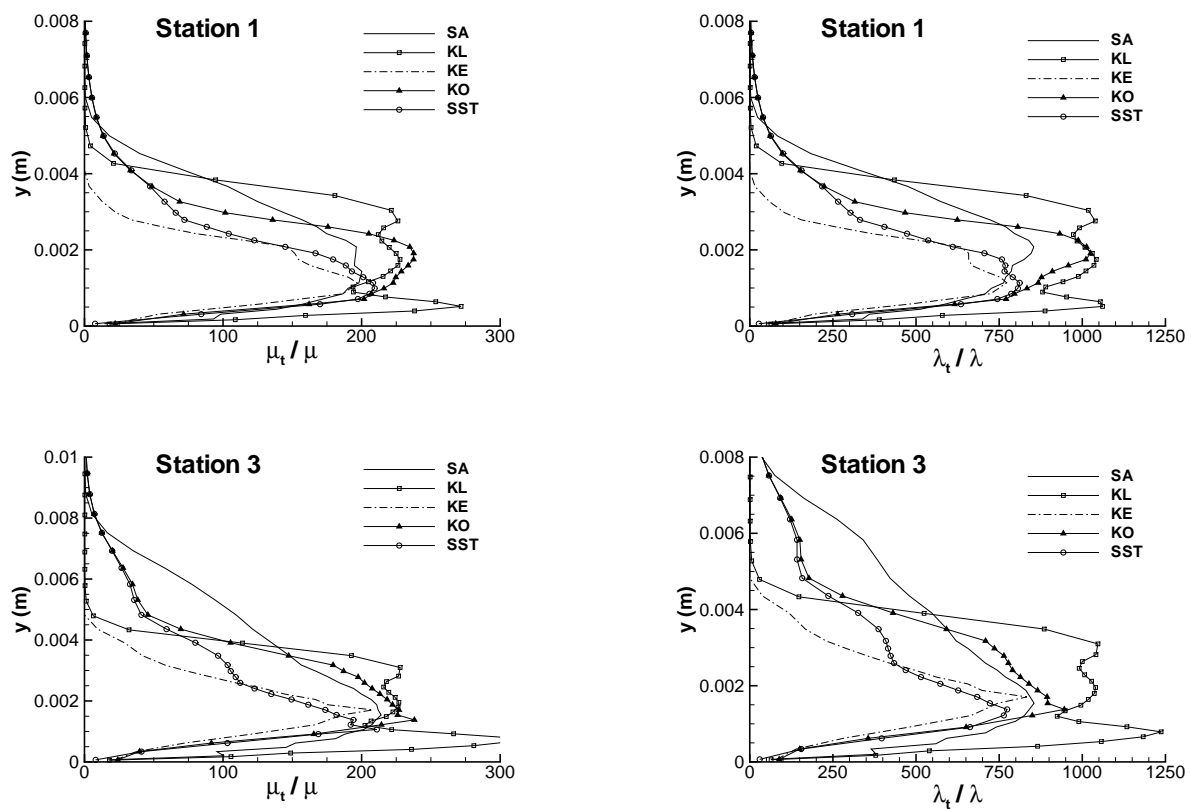


Figure 5: Profiles of ratios μ_t/μ (left) and λ_t/λ (right) at stations 1 and 3, turbulence model influence.

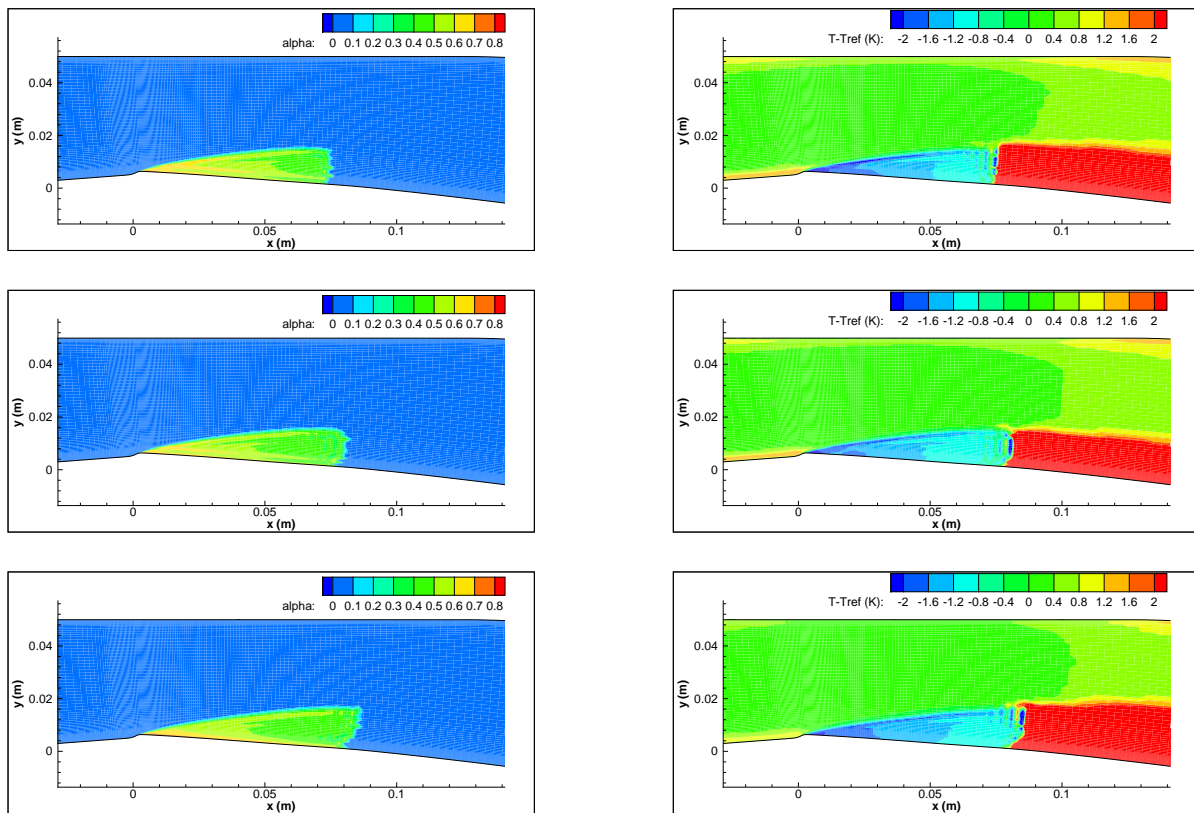


Figure 6: Void ratio (left) and temperature difference $T - T_{ref}$ (K) (right), turbulent Prandtl number influence, $P_{rt} = 1.5$ (top), $P_{rt} = 1$ (middle) and $P_{rt} = 0.25$ (down).

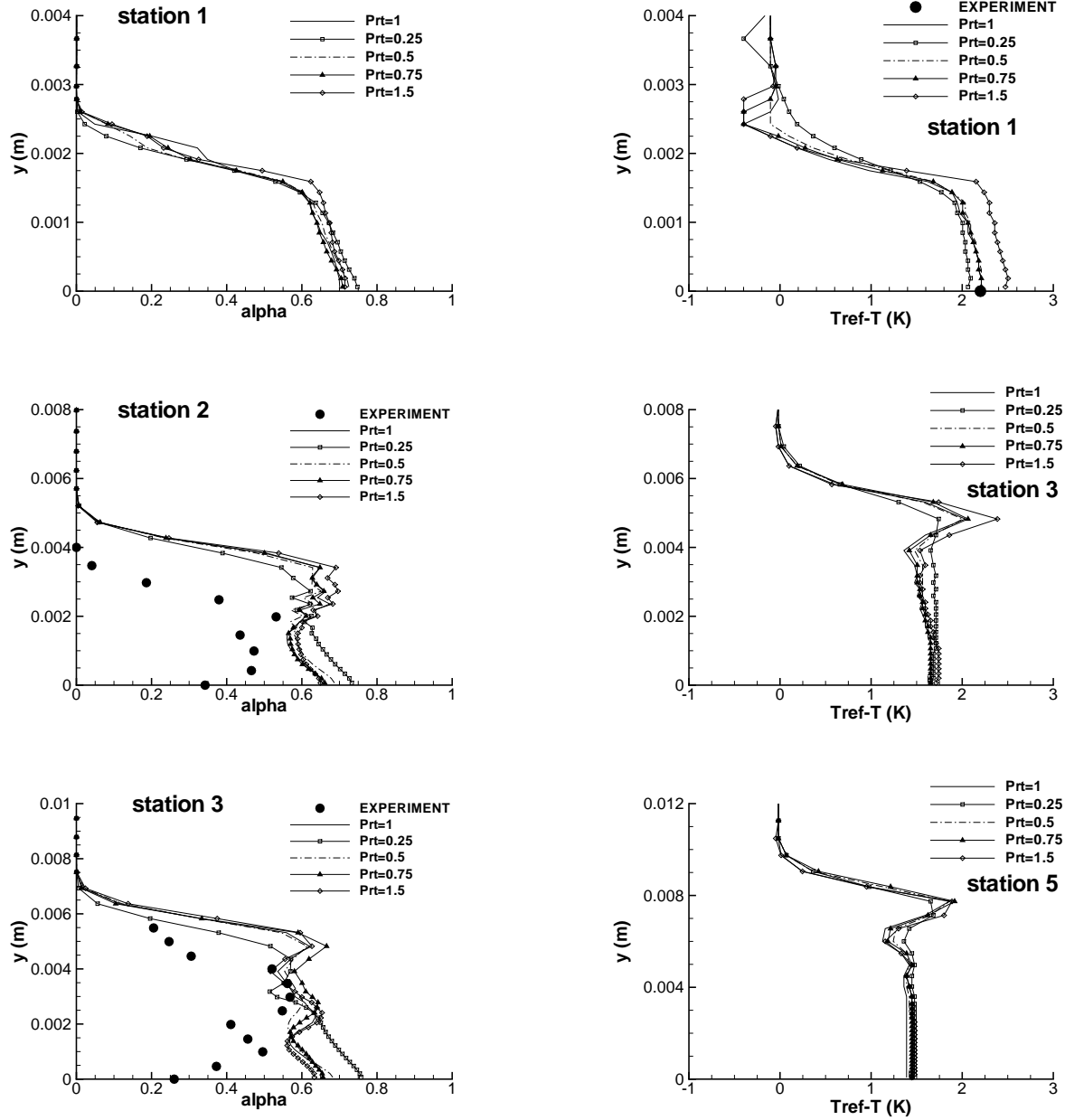


Figure 7: Profiles of void ratio and temperature drop $T_{ref} - T$ at different stations, turbulent Prandtl number influence.

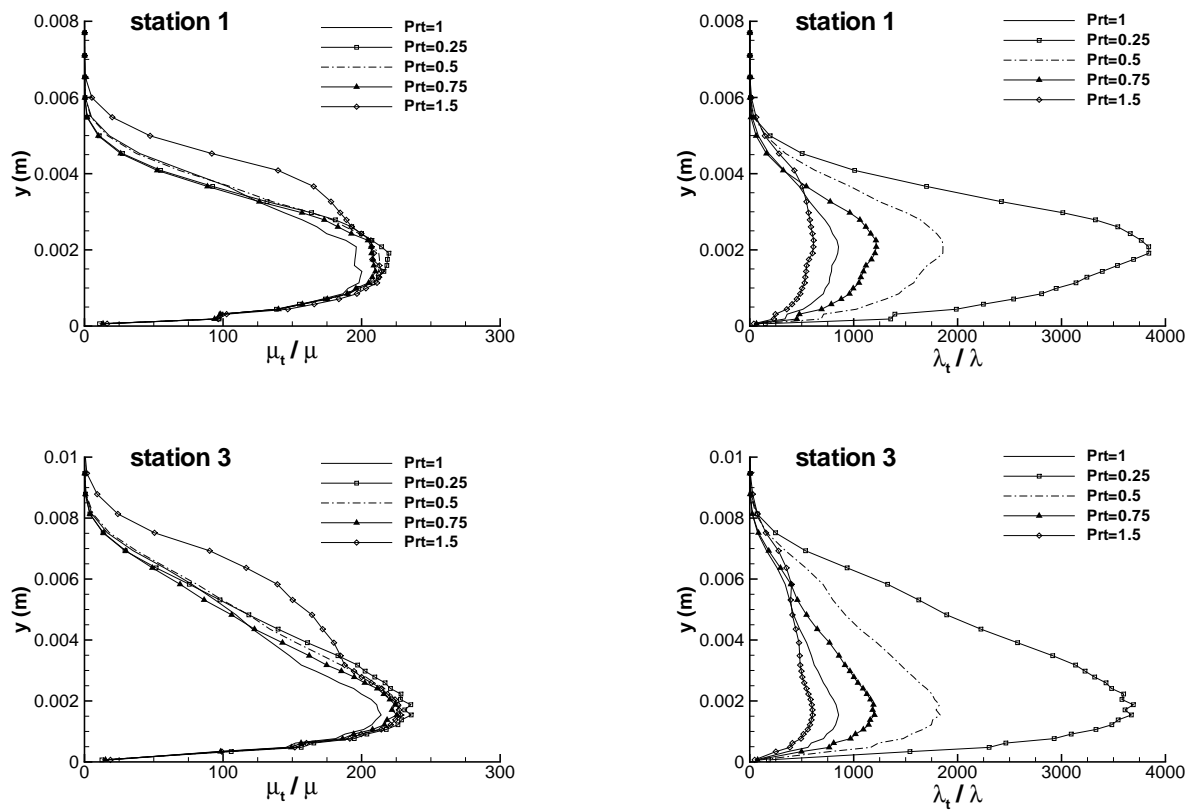


Figure 8: Profiles of ratios μ_t/μ (left) and λ_t/λ (right) at stations 1 and 3, turbulent Prandtl number influence.

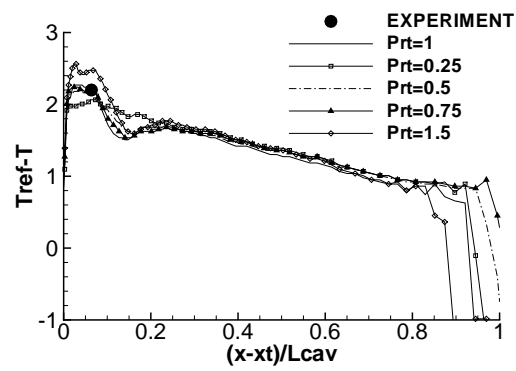


Figure 9: Wall temperature depression $T_{ref}-T$ (K) inside the divergent, turbulent Prandlt number influence.